iScience

CellPress
OPEN ACCESS

Article

Activity modulation of the *Escherichia coli* F_1F_O ATP synthase by a designed antimicrobial peptide via cardiolipin sequestering

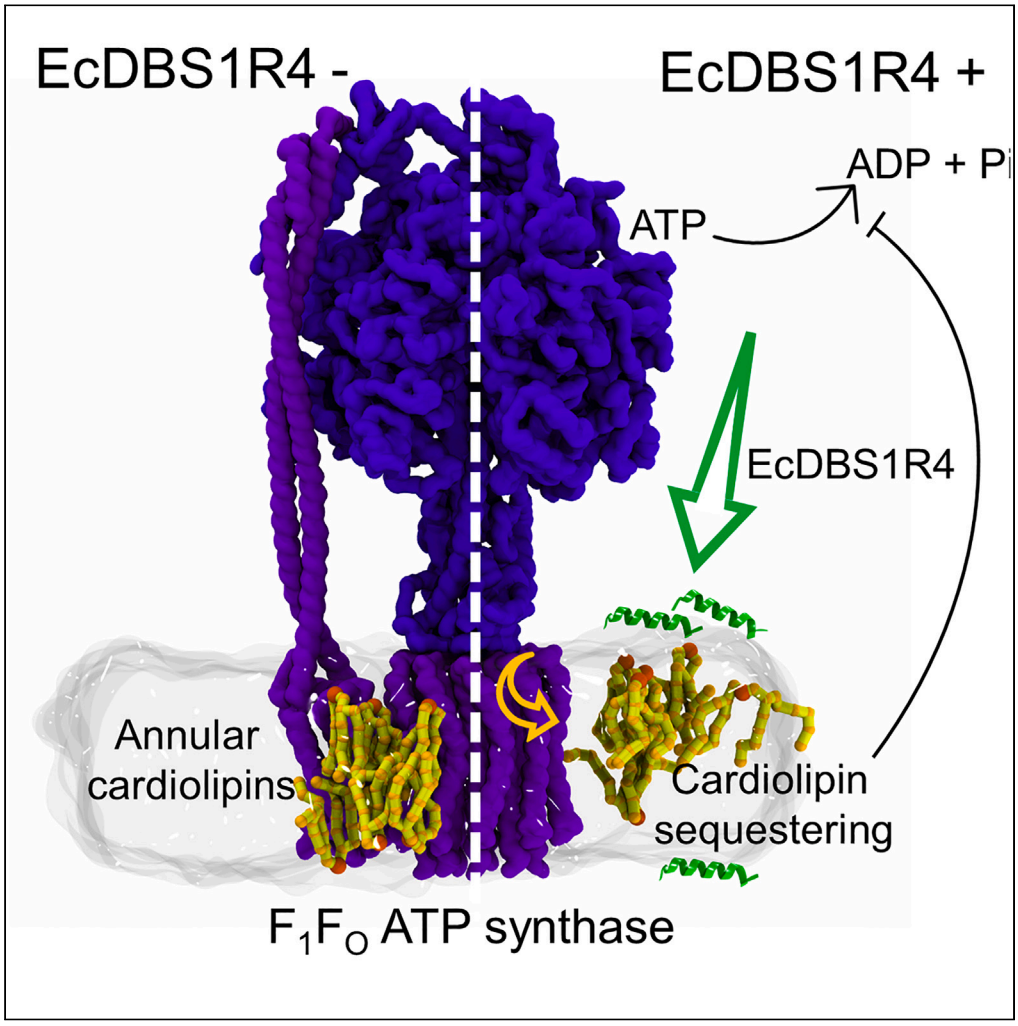

Marcin Makowski, Víctor G. Almendro-Vedia, Marco M. Domingues, Octavio L. Franco, Iván López-Montero, Manuel N. Melo, Nuno C. Santos

ivanlopez@quim.ucm.es (I.L.-M.)
m.n.melo@itqb.unl.pt (M.N.M.)
nsantos@fm.ul.pt (N.C.S.)

Highlights

EcDBS1R4 is an antimicrobial peptide that segregates cardiolipin from other lipids

EcDBS1R4 modulates the activity of ATP synthase in membranes containing cardiolipin

EcDBS1R4 increases hydrophobic mismatching between ATP synthase and the bilayer

EcDBS1R4 sequesters cardiolipin from the interface of ATP synthase

Makowski et al., iScience *26*, 107004
July 21, 2023
https://doi.org/10.1016/j.isci.2023.107004

iScience

CellPress
OPEN ACCESS

Article

Activity modulation of the *Escherichia coli* F_1F_O ATP synthase by a designed antimicrobial peptide via cardiolipin sequestering

Marcin Makowski,[1,2] Víctor G. Almendro-Vedia,[3,4,5] Marco M. Domingues,[1] Octavio L. Franco,[6,7] Iván López-Montero,[3,4,5,*] Manuel N. Melo,[2,*] and Nuno C. Santos[1,8,*]

SUMMARY

Most antimicrobial peptides (AMPs) exert their microbicidal activity through membrane permeabilization. The designed AMP EcDBS1R4 has a cryptic mechanism of action involving the membrane hyperpolarization of *Escherichia coli*, suggesting that EcDBS1R4 may hinder processes involved in membrane potential dissipation. We show that EcDBS1R4 can sequester cardiolipin, a phospholipid that interacts with several respiratory complexes of *E. coli*. Among these, F_1F_O ATP synthase uses membrane potential to fuel ATP synthesis. We found that EcDBS1R4 can modulate the activity of ATP synthase upon partition to membranes containing cardiolipin. Molecular dynamics simulations suggest that EcDBS1R4 alters the membrane environment of the transmembrane F_O motor, impairing cardiolipin interactions with the cytoplasmic face of the peripheral stalk that binds the catalytic F_1 domain to the F_O domain. The proposed mechanism of action, targeting membrane protein function through lipid reorganization may open new venues of research on the mode of action and design of other AMPs.

INTRODUCTION

The global spread of antimicrobial resistance is a public health threat that at its worst, could unfold into a "post-antimicrobial era."[1] The pace at which pathogens acquire resistance is outcompeting the rate of discovery and implementation of new antibiotics. Antimicrobial peptides (AMPs) represent one of the most promising candidates in the fight against antimicrobial resistance.[2] However, despite the high expectations raised by AMPs as a potential source of new antibiotics, a reduced number of formulations have achieved the clinical practice.[3] To reverse this trend, it is paramount to properly understand the mechanism of action that governs the antimicrobial activity of AMPs.

Most AMPs are cationic amphiphiles. The cationic charges of AMPs increase their affinity to the anionic surfaces of bacteria, while amphipathicity renders them prone to interact with lipid bilayers.[4,5] Decades of research have allowed to establish "membrane disruption" as the most common mechanism of action of AMPs.[6] Several models of membrane disruption have been proposed, including membrane bilayer permeabilization through pore formation or via detergent-like mechanisms.[7–10] According to these models, membrane permeabilization would result in the leakage of cytoplasmic solutes and subsequent death of the bacterial cell. Some AMPs, however, show membrane binding but no membranolytic capacity,[11–15] which has led some authors to question the biological significance of the membrane permeabilization paradigm.[16] Also, it has been shown that certain AMPs can alter the lateral organization of lipid bilayers, for instance, by clustering the locally abundant anionic lipids.[17,18] Although lipid segregation has been shown for several antimicrobial peptides, how this can cause bacterial death is harder to envision than the "cytoplasmic leakage" in the membrane permeabilization models.

Lipids interacting with proteins self-organize, giving rise to lateral structure in biomembranes. This lipid lateral organization is required to maintain proper activity of many membrane proteins, evidencing that lipids are much more than a mere solvent for membrane proteins.[19] Membrane proteins seem to interact preferentially with certain lipids, generating a protein-specific membrane environment.[20] Indeed, some lipids are cofactors required for enzyme activity,[21] other can act as chaperones,[22] and other lipids aid in protein oligomerization.[23–25] Furthermore, many membrane proteins require non-lamellar lipids—lipids

[1]Instituto de Medicina Molecular, Faculdade de Medicina, Universidade de Lisboa, 1649-028 Lisbon, Portugal

[2]Instituto de Tecnologia Química e Biológica António Xavier, Universidade Nova de Lisboa, 2780-157 Oeiras, Portugal

[3]Instituto Pluridisciplinar, Universidad Complutense de Madrid, Ps Juan XXIII 1, 28040 Madrid, Spain

[4]Universidad Complutense de Madrid, Departamento de Química Física, 28040 Madrid, Spain

[5]Instituto de Investigación Sanitaria Hospital 12 de Octubre (imas12), 28041 Madrid, Spain

[6]Centro de Análises Proteômicas e Bioquímicas, Pós-graduação em Ciências Genômicas e Biotecnologia, Universidade Católica de Brasília, Brasília, 71966-700 Federal District, Brazil

[7]S-Inova Biotech, Pós-graduação em Biotecnologia, Universidade Católica Dom Bosco, Campo Grande, 79117-900 Mato Grosso do Sul, Brazil

[8]Lead contact

*Correspondence: ivanlopez@quim.ucm.es (I.L.-M.), m.n.melo@itqb.unl.pt (M.N.M.), nsantos@fm.ul.pt (N.C.S.)

https://doi.org/10.1016/j.isci.2023.107004

that coexist in bilayers in a state of curvature frustration—for their assembly and function.[26] Increasing evidence indicates that amphipathic compounds can affect protein function through alteration of bilayer properties such as lateral organization.[27–29] Recently, it has been postulated that antimicrobial peptides could hamper membrane protein function by altering the physical properties of the lipid-bilayer in which they are embedded, which may result in toxicity.[12,30,31]

In this work, we asked whether AMPs could cause lateral lipid redistribution, thereby affecting membrane protein function. To this purpose, we have chosen as a case study a designed AMP named EcDBS1R4 (PMKKKLAARILAKIVAPVW). Previously, we showed that this peptide inhibited the growth of the Gram-negative *Escherichia coli*, causing membrane hyperpolarization.[32] This peptide avidly partitions to lipid vesicle mimics of the inner membrane (IM) of *E. coli*, promoting vesicle aggregation and hemifusion.[32] This suggests an ability to induce redistribution of lateral lipid organization, as required for hemifusion.[33–36] The fusogenic ability of EcDBS1R4 requires the presence of lipids both with negative intrinsic curvature—conic shaped—and with negative charge. Cardiolipin (CL), a lipid that fulfills both requirements, was especially efficient in promoting vesicle fusion. In *E. coli*, CLs make up about 10 wt % of the IM, although this may vary depending on the growth stage.[37] This lipid is circumscribed to the bioenergetic membranes of bacteria and mitochondria, having functional interactions with the electron transport chain complexes of *E. coli*.[38] Therefore, we hypothesized that EcDBS1R4 could impair the activity of these complexes via lateral lipid redistribution, which could explain the observed hyperpolarization effect of this peptide.[32]

To investigate this hypothesis, we have employed a combination of experimental methodologies and molecular dynamics simulations (MD). We show that EcDBS1R4 positions parallel to the bilayer plane, causing important alterations on the bilayer topology, including the formation of CL-rich lipid aggregates. We also found that EcDBS1R4 can modulate the bacterial F_1F_O ATP synthase activity, altering the membrane environment, affecting the lateral distribution of CL.

RESULTS

Membrane remodeling by EcDBS1R4

To investigate the effect of EcDBS1R4 on the lateral lipid diffusion of bilayers containing CL, we used TopFluor-CL as the fluorescent probe in fluorescence recovery after photobleaching (FRAP) experiments (see STAR Methods). We measured lipid diffusion in supported lipid bilayers (SLBs) with two different compositions: pure 1-palmitoyl-2-oleoyl phosphatidylcholine (POPC) and a mixture of POPC/tetra-linoleoyl cardiolipin (CL) (4:1) (Figure 1A). In the absence of peptide, the TopFluor-CL diffusion coefficient (*D*) was significantly higher in POPC/CL (4:1) (1.88×10^{-8} cm^2 s^{-1}) than in POPC bilayers (1.26×10^{-8} cm^2 s^{-1}). Addition of 20 μM of EcDBS1R4 to PC/CL (4:1) SLBs caused an average 6.8-fold drop in the diffusion coefficient, while addition to POPC SLBs caused a 1.9-fold drop (final diffusion coefficients are 2.76×10^{-9} and 6.95×10^{-9} cm^2 s^{-1} for PC:CL (4:1) and POPC, respectively).

Interestingly, in the POPC:CL (4:1) mixture, after approximately 40 min of peptide addition, we observed the appearance of bright TopFluor-CL patches covering approximately 13% of the bilayer (Figure 1B). The bright spots did recover their fluorescence after photobleaching, although recovery was much slower than before the appearance of the bright spots. This implies that new TopFluor-CLs can be recruited to the bright TopFluor-CL-rich patches.

To gain topographic details about these events, we performed atomic force microscopy (AFM) measurements (Figure 1C). We monitored the evolution of the bilayer topography for 98 min, over a 25 μm^2 area. At similar timescales as in the confocal microscopy experiments, we could observe significant alterations in the bilayer structure caused by the peptide, despite the differences in the chemistry of the support (mica in AFM *vs.* silane cushion in confocal microscopy). At times beyond 20 min after peptide addition, we observe that some patches of the bilayer experience a decrease in height. This further evolves into a massive reshaping of the topography of the bilayer. After approximately 45 min of peptide addition, the holes expanded, while the height of intermediate areas remained mostly unaltered (Figure 1C). After approximately 70 min, a fraction of the bilayer lipid gaps became filled with lipid. These "refilled" areas form a flat plateau with frequent bumps, some of them protruding as high as several hundred nanometers (Figure 1D). Our experiments show that the bilayer remodeling activity of EcDBS1R4 in supported bilayers occurs in two phases. In the first stage (< 45 min), EcDBS1R4 carves mostly the exposed leaflet of the bilayer,

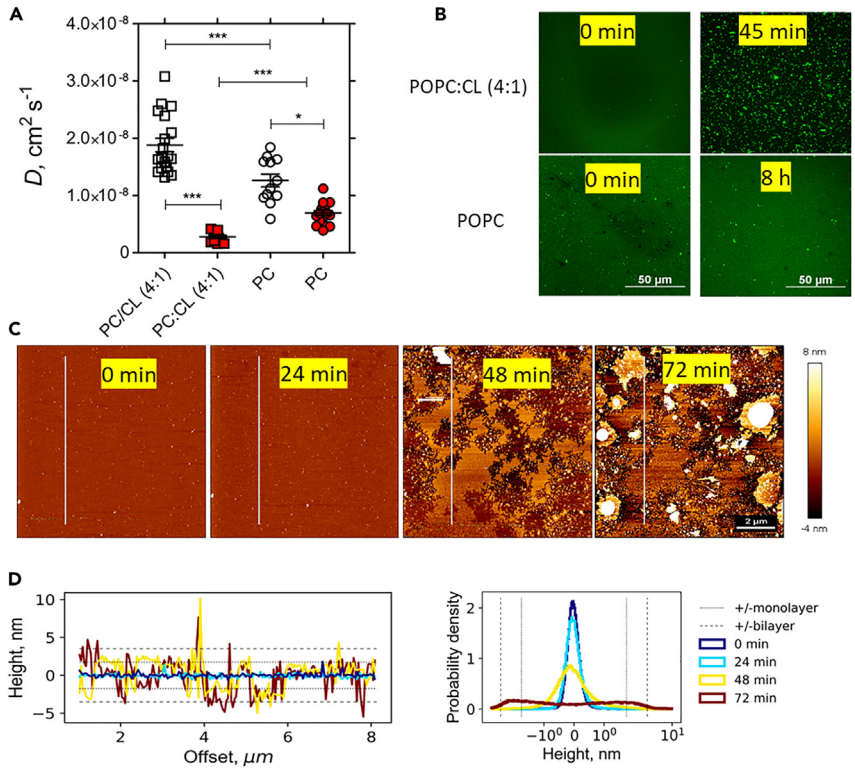

Figure 1. Bilayer remodeling activity by EcDBS1R4

(A) Diffusion coefficient measurements by FRAP of a POPC (circles) and a POPC:CL (4:1) (squares) lipid supported bilayer (lipid concentration of 0.8 mM) in the absence (white) and presence (red) of 20 µM of EcDBS1R4, using 0.5% of TopFluor-CL as the fluorescent probe. *, $p < 0.05$; **, $p < 0.01$ by 1-way ANOVA.

(B) Representative confocal image before and after 45 min of addition of EcDBS1R4 on a POPC:CL (4:1) and a POPC lipid bilayer. The scalebar of the bottom confocal micrograph applies to the confocal micrographs at the top (50 µm).

(C) AFM corrected height images of the time evolution of an incubation with 20 µM of EcDBS1R4 on a PC:CL (4:1) lipid bilayer. The scalebar of the rightmost AFM micrograph applies to the rest of AFM micrographs (2 µm).

(D) Left: the height profile along the white line signaled in C, at three time points; Right: height distribution histogram of the same four time points. The dashed lines in the height profile and height histogram indicate the approximate position of a lipid monolayer (fine dashes) or a lipid bilayer (coarse dashes) below and above the baseline bilayer.

as evidenced by the widening toward the +/− lipid monolayer limits indicated by the fine dashes in the height histogram (Figure 1D yellow line). Then, it promotes the aggregation of lipid in protrusions that can reach over 100 nm.

EcDBS1R4 preferentially locates at curved regions and sequesters cardiolipin

Coarse-grained molecular dynamics simulation studies (see Table 1 for a summary of the simulated systems) were performed aiming at better understanding how EcDBS1R2 affects lipid lateral distribution when interacting with a single leaflet, as it is expected to occur in the SLB experiments. We chose a bicelle, or planar micelle (Figure 2A) as it is a convenient membrane model that allows studying the peptide interacting with only one "leaflet." In our system, a bilayer is built in the *xy*-plane, but with periodic continuity only in *y*. In *x* the discontinuity is filled with water, and the lipid headgroups adapt by forming a curved edge, akin to a bicelle's. In this system, any asymmetric lateral stress exerted by adding the peptide to only one of the "leaflets" can be dissipated by the migration of lipids, around any point along the edges, to the opposite side of the bicelle. A POPC:CL (4:1) mixture and a mixture mimicking the IM composition of *E. coli* were studied.

An initial simulation of a bicelle with dimensions 20 nm × 15 nm, in which the peptide was set free to diffuse, suggested that EcDBS1R4 preferentially positions in the highly curved ends of the bicelle

Table 1. Simulation details

Code name	Lipid composition	F_O motor	Lip:Pep ratio	Replicates[b]
PC:CL (4:1) bicelle	PC:CL (4:1)	No	12:1	1
*Ec*IML bicelle	PE:PG:CL (65:30:5)	No	12:1	1
F_O- | PEP-	PE:PG:CL (65:30:5)	No	N/A	3
F_O- | PEP+	PE:PG:CL (65:30:5)	No	40:1	3
F_O+ | PEP-	PE:PG:CL (65:30:5)	Yes[a]	N/A	3
F_O+ | PEP+	PE:PG:CL (65:30:5)	Yes	40:1	3
F_O+ | PEP+	PE:PG:CL (65:30:5)	Yes	40:1	3

N/A: non applicable (no peptides on the composition).
[a]PDB ID: 6VWK.
[b]Each individual replicate had a total simulation time ≥ 20 μs.

(Figure S1). This is an interesting observation on its own, and hints at membrane perturbation mechanisms by which either buckled or toroidal-pore geometries are stabilized. In our simulations, however, we initially sought to investigate any CL-sequestering ability of the peptide independently of such effects, and employed two corrective restraint strategies: to prevent the peptides from accumulating at the rounded ends of the bicelle, we increased the size of the bicelle (40 nm × 15 nm) and imposed a flat-bottomed harmonic restraint to the peptide's backbone beads, forcing the peptides to remain in a central area—or "corral"—along the *x* axis of the bicelle. This type of potential only acts on peptides leaving the corralled area (being zero, or "flat-bottom," between the corral's limits). Likewise, to prevent buckling—which would have also interfered with the corral strategy—, the entire membrane was subjected to another flat-bottomed potential restraining the lipid acyl-glycerol beads to a *xy* slab 4 nm-thick

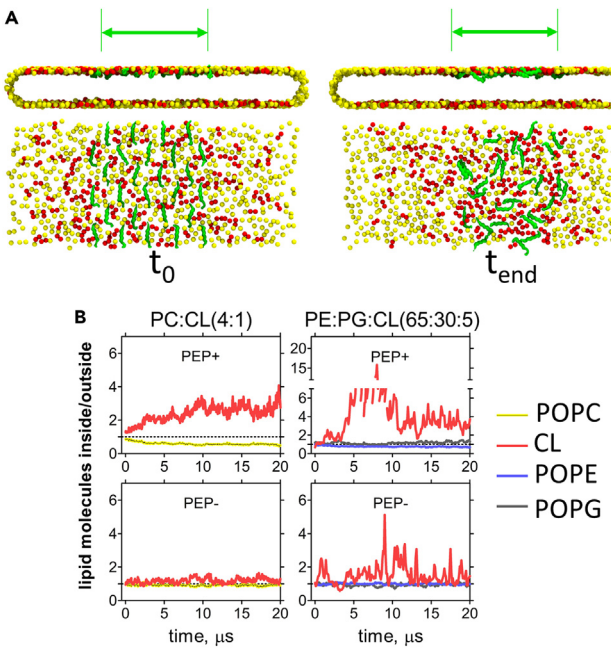

Figure 2. Molecular dynamics simulations of EcDBS1R4 interacting with bicelles containing CL

(A) Snapshots of the top view (top) and side view (bottom) of a POPC:CL (4:1) bicelle on its initial configuration and after 20 μs of simulation. Peptide was added to only one side of the bicelle. For clarity, only the phosphate groups of lipids (yellow: POPC, red: CL) and peptide backbone beads (green) are represented. The green arrows point to the corral borders imposed by a flat-bottomed potential, within which the peptide is forced to stay.

(B) Ratio of lipid distribution inside *vs.* outside the "peptide corral" in a POPC:CL (4:1) and a PE:PG:CL (65:30:5) bilayer (left and right, respectively). Ratios above or below 1 mean enrichment or depletion of a lipid inside the peptide corral, indicating lipid sequestration or exclusion by the peptide. Lipid ratios at the top (PEP+) and bottom (PEP-) leaflets.

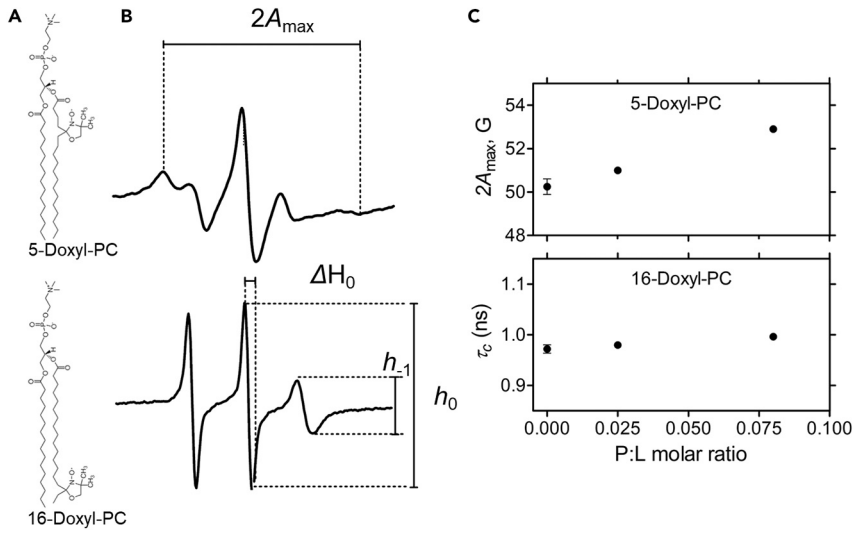

Figure 3. EcDBS1R4 preferential position across the bilayer plane assessed by electron paramagnetic spectroscopy

(A) Chemical structures of the probes used, namely 5-doxyl-PC as the interfacial sensitive probe (reporting close to the bilayer-water interface) and 16-doxyl-PC, sensitive to alterations at the core of the lipid bilayer.

(B) Example of EPR first-derivative absorption spectra of 2.5 mM PC:CL (4:1) + 0.75% spin label (top: 5-doxyl-PC, bottom: 16-doxyl-PC). The spectral parameters used to obtain τ_c are indicated in the 16-doxyl spectrum: h_0, is the mid-field line height; h_{-1}, high-field line height; ΔH_0, mid-field line width; and $2A_{max}$ maximum hyperfine splitting.

(C) Plots of the hyperfine splitting (2Amax) of the 5-doxyl-PC (which is proportional to τ_c), and the rotational times (τ_c) of the 16-doxyl-PC. The τ_c plots show that only 5-doxyl-PC is significantly perturbed by EcDBS1R4, indicating a more interfacial localization of the peptide. Spectra were recorded at 298 K. Error bars indicate standard deviation.

in *z*. We equilibrated the bilayer with embedded peptides for about 6 μs until any lateral strain imposed by the peptides was released—*i.e.*, the distribution of lipid molecules between sides of the bicelle stabilized. We then compared the local lipid concentrations inside and outside the corral area to which the peptides were restricted (see Figure 2A). For the bicelle with composition mimicking that of the IM of *E. coli* (*Ec*IML: 1-palmitoyl-2-oleoyl phosphatidylethanolamine [POPE]: 1-palmitoyl-2-oleoyl phosphatidylglycerol (POPG: CL [65:30:5]), a 4.24-fold relative difference in CL density was observed between the peptide-occupied area and the outside. CL and POPG displaced POPE from the peptide-occupied area (0.76-fold POPE density variation). In the opposite side of the bicelle, lipids were more evenly distributed, although CL was enriched in the area under the corral (1.52-fold density increase). In the POPC:CL (4:1) bilayer, the area inside the peptide corral area was 2.69-fold enriched in CL and depleted in PC (0.54-fold) relative to the peptide-free area (Figure 2B).

EcDBS1R4 positions preferentially parallel to the lipid bilayer plane of CL-containing lipid bilayers

To get insights on how the membrane interacting EcDBS1R4 positions in the lipid bilayer containing CL, we performed electron paramagnetic resonance (EPR) experiments, using two lipids spin labeled either closer to the interfacial region (5-doxyl-PC) or inside the bilayer hydrophobic core (16-doxyl-PC; see Figure 3A). The sensitivity of the doxyl paramagnetic signal to external perturbations is translated into spectral changes—generally, a spectral stretching, or broadening. These spectral changes can be used to investigate alterations in the rotational dynamic timescales (τ_c) that the insertion of the peptide causes at different heights along the normal of the bilayer plane. The spectrum of 16-doxyl-PC remained mostly unaltered, even at high peptide-to-lipid ratios of 1:12 (Figure 3C), with only a very slight alteration in the rotational dynamics (τ_c values of 0.98 and 1.00 in the absence and presence of peptide, respectively). Conversely, the spectrum of the 5-doxyl-PC probe significantly broadens upon addition of peptide, implying that the interaction of EcDBS1R4 with the PC:CL (4:1) lipid bilayer decreases the probe's mobility. This suggests that EcDBS1R4 does not fully penetrate the lipid bilayer, positioning preferentially close to it, parallel to the bilayer plane.

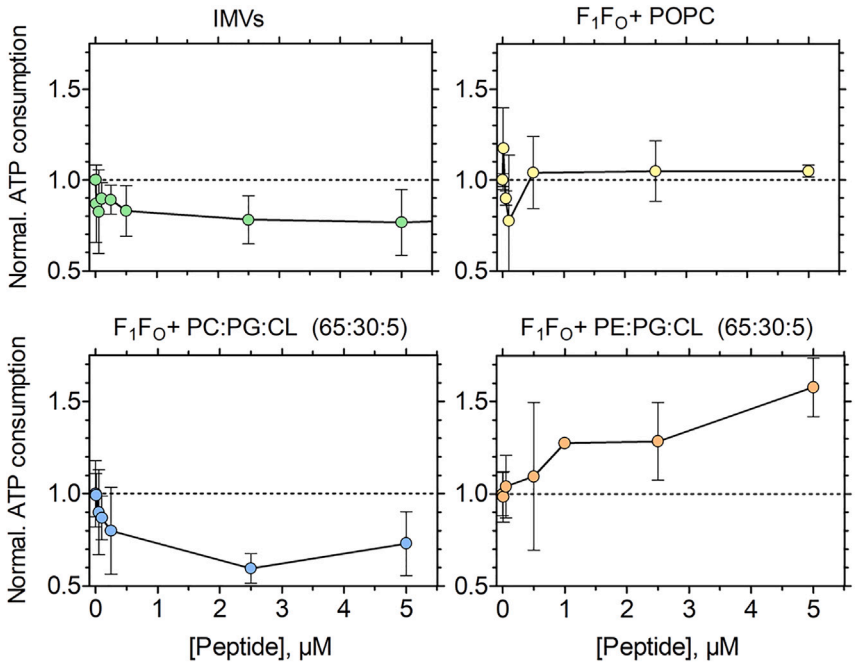

Figure 4. ATPase activity of inner membrane vesicles (IMVs) of *E. coli* and F_1F_0 reconstituted vesicles with different lipid compositions, as a function of EcDBS1R4 concentration

ATPase activity was measured by the colorimetric malachite assay. Lipid concentrations of IMVs (green) and F_1F_O-reconsituted vesicles was 1 mM. The lipid compositions of the reconstituted proteoliposomes were POPC (yellow), POPC:POPG:CL (65:30:5; blue), and POPE:POPG:CL (65:30:5; orange). Each data points represents the average of at least three experiments. Error bars indicate the coefficient of variation.

EcDBS1R4 modulates the F_1F_O ATP synthase activity in CL-containing lipid bilayers

In previous studies, we reported that EcDBS1R4 causes membrane hyperpolarization in *E. coli* cells. We hypothesized that membrane partition of EcDBS1R4 could affect the activity of proteins involved in membrane depolarization such as the F_1F_O ATP synthase. We assessed the ATPase activity of the F_1F_O ATP synthase in the absence and presence of EcDBS1R4 in both IM vesicles (IMVs) of *E. coli* and in model membranes with different phospholipid compositions, by means of the malachite green assay (Figure 4). Peptide addition caused a ~ 20% ATPase activity inhibition of IMVs. Maximum inhibitory activity is already achieved at a peptide concentration of approximately 1 μM. Since IMVs maintain most of the bacterial membrane protein content, including several different proteins with ATPase activity (*e.g.*, ABC transporters), we could not assign the observed inhibitory effect to a specific *E. coli* ATPase. Additionally, we were interested on whether the ability to inhibit the activity of the ATP synthase was lipid-composition dependent and, therefore, a bilayer-mediated process. Thus, we assessed the ATPase activity of F_1F_O proteoliposomes reconstituted in a variety of lipid environments and in the presence of increasing concentrations of EcDBS1R4. POPC:POPG:CL (60:35:5)-F_1F_O proteoliposomes were inhibited by EcDBS1R4 to a similar extent of what was observed for the native IM vesicles. Conversely, the ATPase activity of F_1F_O proteoliposomes prepared without CL in the composition (pure POPC) was not significatively altered by EcDBS1R4. It should be noted that in previous studies, we determined that EcDBS1R4 partitions very poorly to pure POPC bilayers,[32] and thus the lack of inhibitory activity in these proteoliposomes suggests that the ability to modify protein function observed in the other systems is bilayer-mediated and lipid composition-dependent. Surprisingly, EcDBS1R4 increased the ATPase activity in dioleoyl phosphatidylethanolamine (DOPE):POPG:CL (65:30:5) F_1F_O proteoliposomes.

EcDBS1R4 alters the membrane environment of the F_O motor of a bacterial F_1F_O ATP synthase

To explore the effect of EcDBS1R4 on the lipid distribution in a membrane containing an ATP synthase, we performed a series of coarse-grained molecular dynamics simulations. We incorporated an F_O transmembrane domain of the F_OF_1 ATP synthase of *E. coli*[39] (PDB ID: 6VWK) in a membrane with a composition

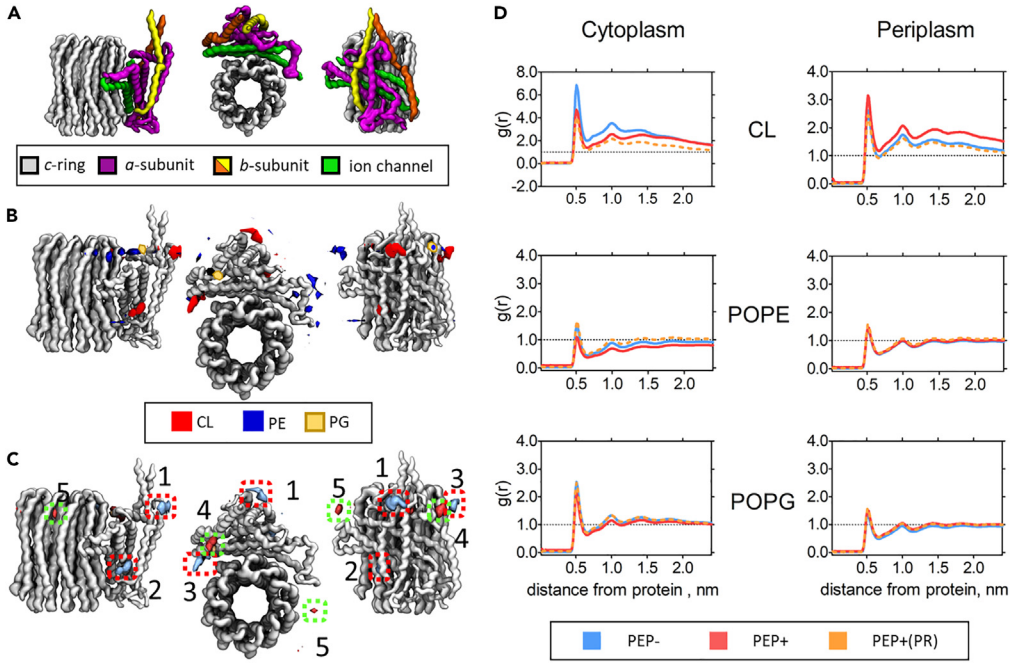

Figure 5. Effects of EcDBS1R4 on the lipid interactions with the F_O motor of *E. coli*

(A) Overview of the structure of the F_O motor of *E. coli*'s ATP synthase (PDB ID: 6VWK). Three views are presented, from left to right: the side view focusing on the *c*-ring; the top view from the cytoplasmic side; and the side view focusing on the *a*-subunit. The main subunits that made up the rotor are color-coded as follows: gray for the *c*-ring; purple for the *a*-subunit; yellow and orange for helices 1 and 2 that conform the *b*-subunit of the peripheral stalk; in green, the two helices perpendicular to the bilayer plane that channel the protons to the *c*-ring.

(B) Occupancy maps of the phosphate residues of each lipid species (red: CL, blue: POPE, and black: POPG) reveal defined lipid territories in the surroundings of the F_O motor.

(C) Occupancy maps of the CL phosphates in the absence of peptide (ice blue), unrestrained peptide (salmon red), and restrained peptide (PEP + (PR); orange). Red and lime dashed highlights represent loss and gain of CL in a territory that is number coded from 1 to 5 for clarity.

(D) Radial distribution functions of lipids in the cytoplasmic and periplasmic leaflets as a function of the distance to the surface of the protein. The color code is shared with C.

similar to the IM of *E. coli*. The different subunits of the F_O motor are depicted in Figure 5A: the *c*-ring, made up by 10 identical subunits; the *a*-subunit, bound to the *c*-ring, bears the ion channel (in green) that fuels the rotation of the *c*-ring; and the *b*-subunits conform the lateral stalk that links the F_O motor with the F_1 soluble motor. Three situations were studied (in triplicate, with a total cumulative simulation time above 200 μs): (i) a control with no peptide; (ii) a simulation with peptide at a lipid-to-peptide ratio of 40:1; (iii) an additional simulation with peptide, in which the peptide backbone beads were restricted from coming within 5.5 nm of the F_O domain's center. This last simulation intended to balance any over-represented peptide-protein interactions due to the reported stickiness of proteins in the Martini 2 model.[40]

Figure 5B shows the time-resolved occupancy maps of the phosphates of each lipid species in the control situation (without peptide). We observe that each lipid species occupies preferentially some defined lipid-specific interfacial interaction regions, or *territories* in the surroundings of the F_O motor. We identified three CL territories: two in the cytoplasmic, and one in the periplasmic side. In the cytoplasmic leaflet, one CL domain is located close to the helices of the *b*-subunit (see Figures 5A and 5B), which makes up the "peripheral stalk" that links the F_O with the F_1 domain. The second CL territory of the cytoplasmic face is located at the interface between the *a*-subunit and the *c*-ring (Figure 5B). POPE molecules tend to position close to the ends of the transversal helices that make up the proton egress channel (in the interface between *a*-subunit and *c*-ring). Finally, there is a territory of the anionic POPG close to the second helix of the *b*-subunit that makes up the peripheral stalk. As for the periplasmic leaflet, a single CL territory is found in the periplasmic leaflet, buried close to the *b*-subunit of the peripheral stalk (Figure 5B).

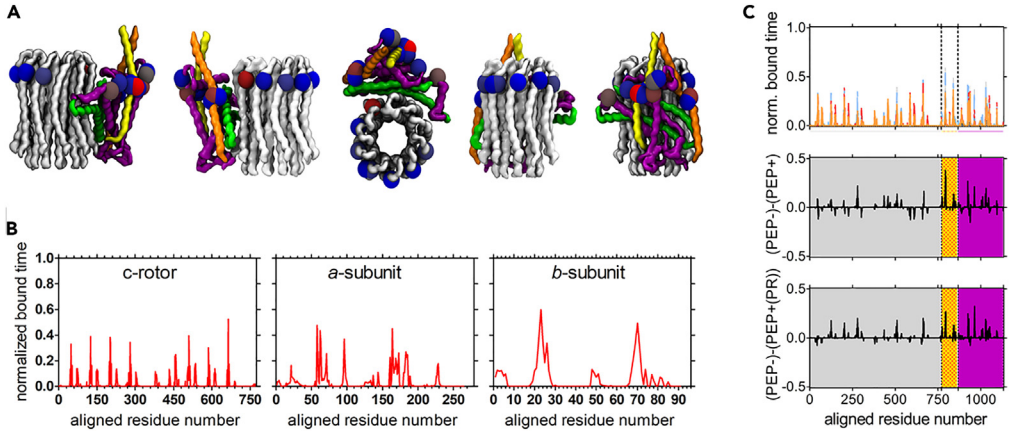

Figure 6. Cardiolipin interactions with the subunits of the F_O motor

(A) Protein-centric view of the most frequent interactions of the F_O motor with CL. The spheres indicate residues that spent at least 30% of the time bound to a CL phosphate bead. The gradient color goes from blue to red, maximum binding is 60% (red residue at *b*-subunit). F_O subunits are color-coded as in Figure 4A.

(B) Normalized total time of CL phosphate-binding to each subunit. Per-subunit break-down of the amino acid residues that participate the most in the binding to CL: *c*-ring: THR 48. *a*-subunit: Ser58, Lys62, Leu96, Met164; *b*-subunit: Tyr 23 (helix 1), Tyr71 (helix 2).

(C) Protein-centric viewpoint of the total time of binding of CL to the F_O motor in the absence and presence of peptide. From top to bottom: normalized bound time of the residues of the F_O motor with the phosphate residues of CL in the absence (ice blue) and presence of unrestricted (salmon red) and restricted peptide (orange); center: difference of normalized binding times between the peptide free simulation and the simulation with unrestrained peptide. Bottom: difference between peptide free and the simulation with restrained peptide. Points above 0 represent residues that interact more with CL in the peptide-free simulation than in the simulation with peptide and vice-versa. Dashed lines represent the boundaries between subunits. The background indicates the different F_O subunits: *c*-ring: gray; *b*-subunit: checkered orange-yellow; *a*-subunit: purple.

To get a glimpse of how membrane interacting EcDBS1R4 may affect the lateral distribution of phospholipids in the proximity of the F_O motor, we calculated the radial distribution function (RDF) of the phosphates of each lipid species as a function of the distance to the protein surface (Figure 5D). RDFs confirm that the annular region of the F_O motor is enriched in CL, when compared to POPE and POPG. CL is particularly abundant among the cytoplasmic annular lipids. Since the occupancy maps suggested that certain subunits in the F_O motor were especially prone to bind CL, we identified the residues that had longer interactions with CL (Figures 6A and 6B). The addition of peptide (either restrained away from F_O or unrestrained) causes considerable depletion of the annular CL in the cytoplasmic leaflet (Figure 5C), particularly in the region of the *b*-subunit (Figure 6C). Conversely, in the periplasmic leaflet, addition of unrestrained peptide increases the density of CL in the surroundings of the F_O, while the restrained peptide does not significantly alter its distribution. The distribution of the annular POPE molecules in the cytoplasmic leaflet is also sensitive to the addition of peptide. While unrestrained peptide causes depletion of POPE, restrained peptide slightly increases its density. The distribution of POPG, on the other hand, is rather insensible to the addition of peptide (Figure 4), suggesting that the sequestering activity of EcDBS1R4 is specific for CL and cannot be attributed exclusively to an electrostatic effect.

EcDBS1R4 affects lipid-protein mismatch and lipid diffusion in bilayers containing the F_O motor of a bacterial F_1F_O ATP synthase

We examined how the peptide influences spatial properties of the bilayer, as these can influence protein function.[19] A naked bilayer (lacking the F_O motor, F_O-) and a naked bilayer to which we added peptide (maintaining the lipid-to-peptide ratio of the F_O+ simulations) were used as controls.

We obtained the lipid diffusion coefficient (*D*) by means of their mean squared displacement. As previous data indicated a pattern of asymmetry between leaflets in the extent of interaction of the lipids with the F_O motor, we measured these coefficients for each leaflet independently. Having embedded F_O lowers the diffusion coefficient of all lipids when compared to the naked bilayer (Figure 7A). Periplasmic CL is the most affected, at a 1.8-fold diffusional slowdown in F_O+ bilayers. Peptide addition to F_O+ bilayers affects

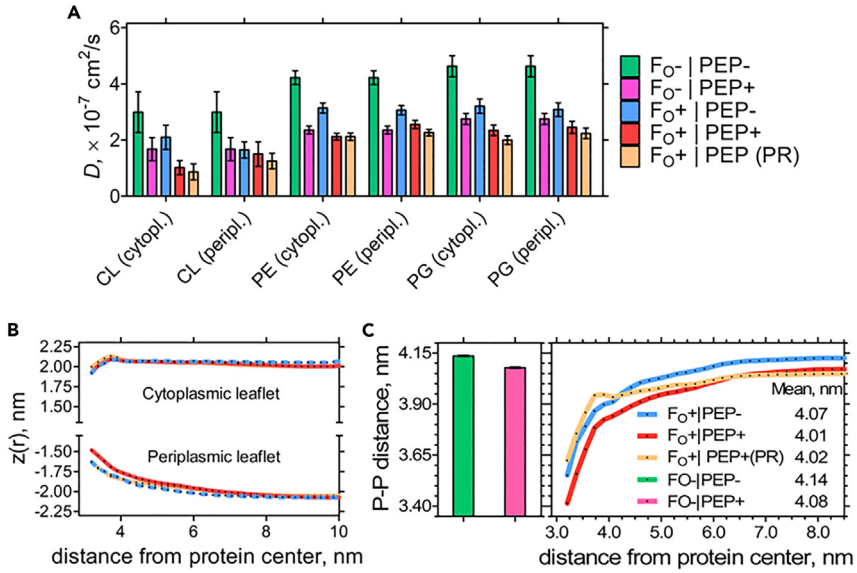

Figure 7. Molecular dynamics studies of the effect of EcDBS1R4 on dynamic and spatial properties of a model bioenergetic membrane

A POPE:POPG:CL (65:30:5) composition was used in all simulated systems: F_O+ systems: bilayers carrying the transmembrane F_O motor of the ATP synthase of *E. coli*; and, F_O- systems: naked bilayers lacking the F_O motor.

(A) Diffusion coefficients of the different lipids.

(B) Average *z*-coordinate position of the phosphate beads of lipids as a function of the distance to the protein center.

(C) Thicknesses of the bilayers measured by the inter-leaflet distance between phosphate beads (P–P distance). On the right, the thickness as a function of the distance to the F_O motor. All simulations were performed in triplicate. Error bars represent the 95% confidence interval.

especially the diffusion of cytoplasmic CL (an approximately 3-fold decrease relative to the naked bilayer diffusion), whereas periplasmic CL is little affected beyond the slowdown brought about by F_O presence. Addition of peptide to either naked or F_O+ bilayers lowers the diffusion coefficient of PE and PG to a lesser extent, similar between the two. Overall, restrained peptide had a slightly higher effect in slowing lipid diffusion than the unrestrained peptide.

Bilayer thickness can affect the supramolecular organization of membrane proteins and their activity.[41] We were thus curious if EcDBS1R2 could affect this parameter in a bilayer with a F_O motor embedded. We measured the distribution of the lipid phosphates along the z-coordinate as a function of the distance from the center of the protein (Figure 7B). The F_O motor causes thinning of the annular lipids when compared to the thickness of the bulk lipids (a 5 Å difference with the bulk lipid thickness). Addition of unrestrained peptide causes further bilayer thinning of the annular lipid region of roughly 1.4 Å, affecting specifically the periplasmic leaflet (Figure 7C). Restrained peptides were unable to affect this annular region.

DISCUSSION

A significant share of our current knowledge regarding antimicrobial peptide activity comes from experiments that have profited from simplistic, yet convenient protein-naked membrane model systems, such as large unilamellar vesicles, supported lipid bilayers, and lipid monolayers. However, cell biomembranes are highly complex, crowded environments, in which the lipid bilayer is densely populated with proteins. Lipids and proteins strongly influence one another. For instance, cytochrome-crowded CL proteoliposomes are immune to the ability of Ca^{2+} to elicit phase transition of CL in naked bilayers.[42] On the other hand, many membrane active peptides are known to alter the lateral distribution of lipids and proteins.[17,18,31] On this basis, we have explored here the effects that this lipid lateral redistribution elicited by an antimicrobial peptide might have on protein function.

The question asked in the present work is whether a cationic amphipathic peptide could modulate membrane protein activity by altering the lipid lateral distribution, causing toxicity. We use as a case study

EcDBS1R4, a designed antimicrobial peptide. In previous studies, we showed that this peptide induces membrane hyperpolarization in *E. coli*. Our results also showed that EcDBS1R4 promoted a composition-dependent vesicle aggregation and hemifusion, suggesting an ability to rearrange lipid lateral distribution. We speculated that EcDBS1R4 might be able to disrupt the activity of proteins involved in membrane potential dissipation, such as F_OF_1 ATP synthase, via lateral lipid reorganization. Our experiments show that EcDBS1R4 has a "bilayer carving" activity in SLBs, akin to both the detergent-like and the anionic lipid clustering models.[9,43] Partition of high concentrations of EcDBS1R4 to PC:CL (4:1) bilayers causes fluorescent TopFluor-CL molecule agglutination in bulky structures that can protrude several hundred nanometers high, as revealed by AFM height measurements. When photobleached, these bright TopFluor-CL-rich aggregates do recover their fluorescence, suggesting that there is a continuum between the bilayer and these spots that allows lipid exchange. Our simulations indicate that this peptide has a CL sequestering ability. CL clustering activity has been previously reported for several mitochondrial proteins[44,45] and, importantly, for the *b*-subunit of *E. coli*'s F_1F_O ATP synthase.[46] In the latter study, authors show that overproduction of *b*-subunit in *E. coli* induces the formation of intracellular membrane structures rich in CL that tend to aggregate in non-lamellar hexagonal phases. We speculate that CL-rich regions induced by EcDBS1R4 could similarly develop into non-lamellar phases responsible for the lipid agglomerates observed by AFM. Furthermore, our simulations using bicelle models also suggest that EcDBS1R4 tends to position itself at highly curved regions of membranes. This may be indicative of a positive feedback chain reaction in which the curved defects in membrane structure attract more peptides that would further increase lipid bilayer damage. The relevance of the lipid-carving activity of EcDBS1R2 beyond the SLBs is questionable. Imaging experiments using giant unilamellar vesicles (GUVs) with vesicles containing CL and high peptide concentrations (L:P molar ratios up to 10:1) revealed vesicle structural stability was apparently intact for longer than 120 min (Figure S2). Interestingly, we were able to capture some events of adhesion and hemifusion, in agreement with previous results,[32] although these were the exception rather than the rule.

We hypothesized that lateral lipid redistribution could affect the activity of proteins related to membrane potential dissipation. To test this hypothesis, we focused on ATP synthase, a protein that uses electrochemical potential dissipation as fuel for ATP synthesis. We show that membrane partitioning of EcDBS1R4 partially inhibits the ATPase activity of F_1F_O ATP synthase of *E. coli*. F_1F_O ATP synthases—as well as other bacterial and eukaryotic respiratory proteins—have known functional interactions with CL.[38,47,48] This inhibitory effect of EcDBS1R4 on the ATPase activity of F_1F_O reconstituted vesicles depends on the lipid composition of the reconstituted vesicles. F_1F_O reconstituted vesicles lacking CL were unaffected by the peptide. It seems thus reasonable to speculate that the enzyme inhibition depends on an indirect membrane-mediated interaction of the peptide, rather than the inhibition *via* binding to the F_1 soluble fraction of the ATP synthase, as it has been proposed for other antimicrobial peptides.[49,50] Interestingly, EcDBS1R4 stimulated ATPase activity of F_1F_O reconstituted in PE:PG:CL vesicles. We attribute this effect to a lower structural stability of these bilayers due to the high content of lipids that induce intrinsic curvature (PE, CL), as opposed to the typically lamellar POPC, associated with planar membranes, but this hypothesis needs validation.

Our simulations indicate that each lipid species locates preferentially within defined territories around the F_O motor of the ATP synthase.[20] The most enriched lipid in the proximity of the F_O motor is CL, in agreement with previous claims.[51,52] The distribution of annular CL is asymmetric, higher in the cytoplasmic than in the periplasmic leaflet. However, cytoplasmic CL diffused faster than the periplasmic ones, suggesting that the interactions with the F_O motor are frequent but transient, similarly to what was previously reported for the metazoan *c*-ring of ATP synthase.[51] We identify two CL territories in proximity to the dimer of the *b*-subunit—the "peripheral stalk" that links the F_O and F_1 motors. The herein reported CL territories close to the *b*-subunit, along with previous observations in mitochondrial ATP synthase in diverse organisms,[52,53] strongly suggest a widely conserved interaction with functional implications. For mitochondrial ATP synthases, structural studies suggest that CL binding to the *b*-subunit aids in the oligomerization of ATP synthase into dimers and superior oligomers and in the stabilization of the motor.[52,54] However, no bacterial ATP synthase dimers have been found to date. This suggests additional functions for CL in the membrane environment of the F_1F_O ATP synthase. It has been argued that bacterial membranes are enriched in lipids with negative curvature, such as CL, to maintain the functionality of membrane proteins, stabilizing their membrane embedding.[19,26,55] Our observations are in line with this view in that the behavior of annular CLs is compatible with a stabilization of the irregular, bumpy surface of the transmembrane F_O motor.

EcDBS1R4 displaces CL from the surroundings of the F_O motor. Our lipid occupancy maps allowed pinpointing specific sites of depletion, including the CL territories in the vicinity of the *b*-subunit. By hampering the interaction with these conserved CL, EcDBS1R4 might imbalance the conformational equilibria of the F_1F_O ATP synthase.[56] Moreover, EcDBS1R4 altered lipid diffusion and spatial properties of the lipid bilayer. The peptide has a higher effect on the diffusion of CL than on any other lipid. According to previous claims, CL has transient but frequent interactions with the *c*-ring of metazoan ATP synthases, a feature that was attributed to a lubricative property of CL. The decrease in CL diffusion caused by EcDBS1R4 could impair this alleged lubricant activity of CL, which in turn could hamper the rotation of the *c*-ring.[51] However, our simulations also indicate that the preferred sites of interaction of CL are the concavities of the *a*- and *b*-subunits. Moreover, our simulations indicate that EcDBS1R4 affects the protein-bilayer hydrophobic mismatch and the packing of annular lipids. EcDBS1R4 causes a 5 Å decrease in bilayer thickness, a parameter that has been previously identified as a modulator of ATP synthase activity.[57] Thickness differences of such magnitude in the hydrophobic mismatch rarely cause protein aggregation, and can be locally compensated by lipid chain order adaptations.[58] Such alterations on bilayer thickness could affect the rotatory dynamics and stability of the F_O motor, leading to alterations in the protein activity.

Finally, CL has known interactions with many proteins of *E. coli* besides ATP synthase. Among these, not only a variety of proteins involved in aerobic, anaerobic, and fermentative metabolism,[59] but also proteins involved in a variety of functions, such as osmotic stress response, aquaporins, actin homologs, solute transporters, or mechanosensitive proteins.[23,48,56,60–62] In this work, we focused on the effects of the EcDBS1R4 AMP on F_1F_O due to its central role in respiratory metabolism (either anaerobic or aerobic) and membrane potential dissipation of *E. coli*. We arrived at strong mechanistic observations linking EcDBS1R4 activity to its perturbation of F_1F_O via interaction with the membrane—particularly with CL. Beyond a mere understanding of EcDSB1R2 action, our mechanistic hypotheses may open new directions to understand how CL sequestering can affect the activity of these proteins. Ultimately, this can pave the way for novel therapeutic strategies, for instance by providing templates for the design of new amphipathic peptides able to modulate protein activity via lipid-protein interaction interference. It should be noticed that CL is a prevalent lipid among bacteria, and thus, CL sequestration might be used not only against *E. coli*, but also to fight other bacterial pathogens. Furthermore, future experiments may aim at testing if other AMPs that induce membrane hyperpolarization, such as guavanin-1,[14] PMP-1, and combinations of colistin and tobramycin[13] also act through a lipid bilayer-based disruption of the pathogen's respiratory machinery. As several AMPs have also anticancer properties,[63] and considering that mitochondrial membranes are rich in CL, it is fair to question whether EcDBS1R4 would affect the mitochondria of cancer cells (alone or in combination with other drugs) through a homologous mechanism.

Limitations of the study

This study has some limitations, which we acknowledge. The protein-to-lipid ratio in the experiments for the F_1F_O proteoliposomes is low, while *E. coli*'s plasma membrane is absolutely crowded. We chose a low ratio in order to minimize the possible effects that inter-F_O interactions could have on the accessibility of the peptide to the protein-lipid interface. Additionally, for the sake of simplicity, the setup of our simulations includes peptide molecules interacting with both the inner (cytoplasmic) and outer (periplasmic) leaflets of model membranes of the IM of *E. coli*. Most of the observed effects of EcDBS1R2 take place at the cytoplasmic leaflet. However, it is not clear how or if EcDBS1R2 efficiently translocates to the inner leaflet in bacterial membranes. Moreover, we cannot disregard the possibility of EcDBS1R4 acting as a wedge, blocking the rotary *c*-ring of F_O.

STAR★METHODS

Detailed methods are provided in the online version of this paper and include the following:

- KEY RESOURCES TABLE
- RESOURCE AVAILABILITY
  - Lead contact
  - Materials availability
  - Data and code availability
- EXPERIMENTAL MODEL AND STUDY PARTICIPANT DETAILS
  - Bacteria strains and culture
- METHOD DETAILS

SUPPLEMENTAL INFORMATION

Supplemental information can be found online at https://doi.org/10.1016/j.isci.2023.107004.

ACKNOWLEDGMENTS

This work was supported by Fundação para a Ciência e a Tecnologia—Ministério da Ciência, Tecnologia e Ensino Superior (FCT-MCTES, Portugal), including project 2022.01991.PTDC. M.M. acknowledges financial support from FCT-MCTES fellowship SPRH/BD/128290/2017, and European Molecular Biology Organization—EMBO short-term fellowship number 8558. M.N.M. thanks FCT-MCTES for contract CEECIND/04124/2017. I.L.-M. acknowledges financial support from the Spanish Ministry of Science, Innovation and Universities through the grant PGC2018-097903-B-I00, and the TECNOLOGÍAS 2018 program funded by the Regional Government of Madrid (Grant S2018/BAA-4403 SINOXPHOS-CM). Authors acknowledge the CAI (Centro de Asistencia a la Investigación) Técnicas Químicas - Unidad de Resonancia Magnética of the Universidad Complutense de Madrid for the Electron Paramagnetic Resonsance measurements. O.L.F. acknwoledges support from the Brazilian funding agencies Fundação de Apoio ao Desenvolvimento do Ensino, Ciência e Tecnologia do Estado de Mato Grosso do Sul (FUNDECT), Fundação de Apoio à Pesquisa do Distrito Federal (FAPDF), Coordenação de Aperfeiçoamento de Pessoal de Nível Superior (CAPES) and Conselho Nacional de Desenvolvimento Científico e Tecnológico (CNPq).

AUTHOR CONTRIBUTIONS

M.M.: Conceptualization, formal analysis, investigation, writing—original draft, visualization; V.G.A.V.: investigation, writing—review and editing; M.M.D.: investigation; O.L.F.: writing: review and editing, resources; I.L.-M.: resources, supervision, writing—review and editing; M.N.M.: resources, investigation, software, supervision, writing—review and editing; N.C.S.: resources, supervision, funding acquisition, writing—review and editing.

DECLARATION OF INTERESTS

Authors declare no competing interests.

Received: September 6, 2022
Revised: February 13, 2023
Accepted: May 26, 2023
Published: May 30, 2023

REFERENCES

1. Reardon, S. (2014). WHO warns against "post-antibiotic" era. Nature. https://doi.org/10.1038/nature.2014.15135.

2. Lakshmaiah Narayana, J., and Chen, J.Y. (2015). Antimicrobial peptides: possible anti-infective agents. Peptides *72*, 88–94. https://doi.org/10.1016/j.peptides.2015.05.012.

3. Mahlapuu, M., Håkansson, J., Ringstad, L., and Björn, C. (2016). Antimicrobial peptides: an emerging category of therapeutic agents. Front. Cell. Infect. Microbiol. *6*, 194. https://doi.org/10.3389/fcimb.2016.00194.

4. Fjell, C.D., Hiss, J.A., Hancock, R.E.W., and Schneider, G. (2011). Designing antimicrobial peptides: form follows function. Nat. Rev. Drug Discov. *11*, 37–51. https://doi.org/10.1038/nrd3591.

5. Sani, M.A., and Separovic, F. (2016). How membrane-active peptides get into lipid membranes. Acc. Chem. Res. *49*, 1130–1138. https://doi.org/10.1021/acs.accounts.6b00074.

6. Sato, H., and Feix, J.B. (2006). Peptide-membrane interactions and mechanisms of membrane destruction by amphipathic α-helical antimicrobial peptides. Biochim. Biophys. Acta *1758*, 1245–1256. https://doi.org/10.1016/j.bbamem.2006.02.021.

7. Yang, L., Harroun, T.A., Weiss, T.M., Ding, L., and Huang, H.W. (2001). Barrel-stave model or toroidal model? A case study on melittin pores. Biophys. J. *81*, 1475–1485. https://doi.org/10.1016/S0006-3495(01)75802-X.

8. Matsuzaki, K., Murase, O., Fujii, N., and Miyajima, K. (1996). An antimicrobial peptide, magainin 2, induced rapid flip-flop of phospholipids coupled with pore formation and peptide translocation. Biochemistry *35*, 11361–11368. https://doi.org/10.1021/bi960016v.

9. Bechinger, B., and Lohner, K. (2006). Detergent-like actions of linear amphipathic cationic antimicrobial peptides. Biochim. Biophys. Acta *1758*, 1529–1539. https://doi.org/10.1016/j.bbamem.2006.07.001.

10. Sansom, M.S. (1991). The biophysics of peptide models of ion channels. Prog. Biophys. Mol. Biol. *55*, 139–235. https://doi.org/10.1016/0079-6107(91)90004-C.

11. Wu, M., Maier, E., Benz, R., and Hancock, R.E. (1999). Mechanism of interaction of different classes of cationic antimicrobial peptides with planar bilayers and with the cytoplasmic membrane of *Escherichia coli*. Biochemistry *38*, 7235–7242. https://doi.org/10.1021/bi9826299.

12. Spindler, E.C., Hale, J.D.F., Giddings, T.H., Hancock, R.E.W., and Gill, R.T. (2011). Deciphering the mode of action of the synthetic antimicrobial peptide bac8c. Antimicrob. Agents Chemother. *55*, 1706–1716. https://doi.org/10.1128/AAC.01053-10.

13. Kashyap, S., Kaur, S., Sharma, P., and Capalash, N. (2021). Combination of colistin and tobramycin inhibits persistence of *Acinetobacter baumannii* by membrane hyperpolarization and down-regulation of efflux pumps. Microb. Infect. *23*, 104795. https://doi.org/10.1016/j.micinf.2021.104795.

14. Porto, W.F., Irazazabal, L., Alves, E.S.F., Ribeiro, S.M., Matos, C.O., Pires, Á.S., Fensterseifer, I.C.M., Miranda, V.J., Haney, E.F., Humblot, V., et al. (2018). In silico optimization of a guava antimicrobial peptide enables combinatorial exploration for peptide design. Nat. Commun. *9*, 1490. https://doi.org/10.1038/s41467-018-03746-3.

15. Li, W., O'Brien-Simpson, N.M., Tailhades, J., Pantarat, N., Dawson, R.M., Otvos, L., Reynolds, E.C., Separovic, F., Hossain, M.A., and Wade, J.D. (2015). Multimerization of a proline-rich antimicrobial peptide, Chex-Arg20, alters its mechanism of interaction with the Escherichia coli membrane. Chem. Biol. *22*, 1250–1258. https://doi.org/10.1016/j.chembiol.2015.08.011.

16. Wimley, W.C. (2010). Describing the mechanism of antimicrobial peptide action with the interfacial activity model. ACS Chem. Biol. *5*, 905–917. https://doi.org/10.1021/cb1001558.

17. Sharma, V.K., and Qian, S. (2019). Effect of an antimicrobial peptide on lateral segregation of lipids: a structure and dynamics study by neutron scattering. Langmuir *35*, 4152–4160. https://doi.org/10.1021/acs.langmuir.8b04158.

18. Wadhwani, P., Epand, R.F., Heidenreich, N., Bürck, J., Ulrich, A.S., and Epand, R.M. (2012). Membrane-active peptides and the clustering of anionic lipids. Biophys. J. *103*, 265–274. https://doi.org/10.1016/j.bpj.2012.06.004.

19. Lee, A.G. (2004). How lipids affect the activities of integral membrane proteins. Biochim. Biophys. Acta *1666*, 62–87. https://doi.org/10.1016/j.bbamem.2004.05.012.

20. Corradi, V., Mendez-Villuendas, E., Ingólfsson, H.I., Gu, R.X., Siuda, I., Melo, M.N., Moussatova, A., DeGagné, L.J., Sejdiu, B.I., Singh, G., et al. (2018). Lipid-protein interactions are unique fingerprints for membrane proteins. ACS Cent. Sci. *4*, 709–717. https://doi.org/10.1021/acscentsci.8b00143.

21. Guskov, A., Kern, J., Gabdulkhakov, A., Broser, M., Zouni, A., and Saenger, W. (2009). Cyanobacterial photosystem II at 2.9-Å resolution and the role of quinones, lipids, channels and chloride. Nat. Struct. Mol. Biol. *16*, 334–342. https://doi.org/10.1038/nsmb.1559.

22. Dowhan, W., and Bogdanov, M. (2009). Lipid-dependent membrane protein topogenesis. Annu. Rev. Biochem. *78*, 515–540. https://doi.org/10.1146/annurev.biochem.77.060806.091251.

23. Gupta, K., Donlan, J.A.C., Hopper, J.T.S., Uzdavinys, P., Landreh, M., Struwe, W.B., Drew, D., Baldwin, A.J., Stansfeld, P.J., and Robinson, C.V. (2017). The role of interfacial lipids in stabilizing membrane protein oligomers. Nature *541*, 421–424. https://doi.org/10.1038/nature20820.

24. Raja, M. (2010). The role of phosphatidic acid and cardiolipin in stability of the tetrameric assembly of potassium channel KcsA. J. Membr. Biol. *234*, 235–240. https://doi.org/10.1007/s00232-010-9251-8.

25. Betaneli, V., Petrov, E.P., and Schwille, P. (2012). The role of lipids in VDAC oligomerization. Biophys. J. *102*, 523–531. https://doi.org/10.1016/j.bpj.2011.12.049.

26. Brown, M.F. (2012). Curvature forces in membrane lipid-protein interactions. Biochemistry *51*, 9782–9795. https://doi.org/10.1021/bi301332v.

27. Ingólfsson, H.I., Thakur, P., Herold, K.F., Hobart, E.A., Ramsey, N.B., Periole, X., De Jong, D.H., Zwama, M., Yilmaz, D., Hall, K., et al. (2014). Phytochemicals perturb membranes and promiscuously alter protein function. ACS Chem. Biol. *9*, 1788–1798. https://doi.org/10.1021/cb500086e.

28. Sun, D., Peyear, T.A., Bennett, W.F.D., Holcomb, M., He, S., Zhu, F., Lightstone, F.C., Andersen, O.S., and Ingólfsson, H.I. (2020). Assessing the perturbing effects of drugs on lipid bilayers using gramicidin channel-based in silico and in vitro assays. J. Med. Chem. *63*, 11809–11818. https://doi.org/10.1021/acs.jmedchem.0c00958.

29. Melo, M.N., Arnarez, C., Sikkema, H., Kumar, N., Walko, M., Berendsen, H.J.C., Kocer, A., Marrink, S.J., and Ingólfsson, H.I. (2017). High-throughput simulations reveal membrane-mediated effects of alcohols on MscL gating. J. Am. Chem. Soc. *139*, 2664–2671. https://doi.org/10.1021/jacs.6b11091.

30. Hamoen, L.W., and Wenzel, M. (2017). Editorial: antimicrobial peptides - interaction with membrane lipids and proteins. Front. Cell Dev. Biol. *5*, 4. https://doi.org/10.3389/fcell.2017.00004.

31. Wenzel, M., Chiriac, A.I., Otto, A., Zweytick, D., May, C., Schumacher, C., Gust, R., Albada, H.B., Penkova, M., Krämer, U., et al. (2014). Small cationic antimicrobial peptides delocalize peripheral membrane proteins. Proc. Natl. Acad. Sci. USA *111*, E1409–E1418. https://doi.org/10.1073/pnas.1319900111.

32. Makowski, M., Felício, M.R., Fensterseifer, I.C.M., Franco, O.L., Santos, N.C., and Gonçalves, S. (2020). EcDBS1R4, an antimicrobial peptide effective against Escherichia coli with in vitro fusogenic ability. Int. J. Mol. Sci. *21*, 9104. https://doi.org/10.3390/ijms21239104.

33. Tsai, H.-H.G., Lai, W.-X., Lin, H.-D., Lee, J.-B., Juang, W.-F., and Tseng, W.-H. (2012). Molecular dynamics simulation of cation–phospholipid clustering in phospholipid bilayers: possible role in stalk formation during membrane fusion. Biochim. Biophys. Acta *1818*, 2742–2755. https://doi.org/10.1016/J.BBAMEM.2012.05.029.

34. Henriques, S.T., and Castanho, M.A.R.B. (2004). Consequences of nonlytic membrane perturbation to the translocation of the cell penetrating peptide pep-1 in lipidic vesicles. Biochemistry *43*, 9716–9724. https://doi.org/10.1021/bi036325k.

35. Haney, E.F., Nathoo, S., Vogel, H.J., and Prenner, E.J. (2010). Induction of non-lamellar lipid phases by antimicrobial peptides: a potential link to mode of action. Chem. Phys. Lipids *163*, 82–93. https://doi.org/10.1016/j.chemphyslip.2009.09.002.

36. Stepanyants, N., Macdonald, P.J., Francy, C.A., Mears, J.A., Qi, X., and Ramachandran, R. (2015). Cardiolipin's propensity for phase transition and its reorganization by dynamin-related protein 1 form a basis for mitochondrial membrane fission. Mol. Biol. Cell *26*, 3104–3116. https://doi.org/10.1091/mbc.E15-06-0330.

37. Cronan, J.E., Jr. (1968). Phospholipid alterations during growth of Escherichia coli. J. Bacteriol. *95*, 2054–2061. https://doi.org/10.1128/jb.95.6.2054-2061.1968.

38. Arias-Cartin, R., Grimaldi, S., Pommier, J., Lanciano, P., Schaefer, C., Arnoux, P., Giordano, G., Guigliarelli, B., and Magalon,

A. (2011). Cardiolipin-based respiratory complex activation in bacteria. Proc. Natl. Acad. Sci. USA *108*, 7781–7786. https://doi.org/10.1073/pnas.1010427108.

39. Sobti, M., Walshe, J.L., Wu, D., Ishmukhametov, R., Zeng, Y.C., Robinson, C.V., Berry, R.M., and Stewart, A.G. (2020). Cryo-EM structures provide insight into how *E. coli* F_1F_o ATP synthase accommodates symmetry mismatch. Nat. Commun. *11*, 2615. https://doi.org/10.1038/s41467-020-16387-2.

40. Alessandri, R., Souza, P.C.T., Thallmair, S., Melo, M.N., De Vries, A.H., and Marrink, S.J. (2019). Pitfalls of the martini model. J. Chem. Theor. Comput. *15*, 5448–5460. https://doi.org/10.1021/acs.jctc.9b00473.

41. Kahraman, O., Koch, P.D., Klug, W.S., and Haselwandter, C.A. (2016). Bilayer-thickness-mediated interactions between integral membrane proteins. Phys. Rev. E *93*, 042410–042486. https://doi.org/10.1103/PhysRevE.93.042410.

42. Rietveld, A., van Kemenade, T.J., Hak, T., Verkleij, A.J., and de Kruijff, B. (1987). The effect of cytochrome c oxidase on lipid polymorphism of model membranes containing cardiolipin. Eur. J. Biochem. *164*, 137–140. https://doi.org/10.1111/j.1432-1033.1987.tb11004.x.

43. Epand, R.M., and Epand, R.F. (2009). Lipid domains in bacterial membranes and the action of antimicrobial agents. Biochim. Biophys. Acta *1788*, 289–294. https://doi.org/10.1016/j.bbamem.2008.08.023.

44. Maniti, O., Cheniour, M., Lecompte, M.F., Marcillat, O., Buchet, R., Vial, C., and Granjon, T. (2011). Acyl chain composition determines cardiolipin clustering induced by mitochondrial creatine kinase binding to monolayers. Biochim. Biophys. Acta *1808*, 1129–1139. https://doi.org/10.1016/j.bbamem.2011.01.005.

45. Epand, R.F., Tokarska-Schlattner, M., Schlattner, U., Wallimann, T., and Epand, R.M. (2007). Cardiolipin clusters and membrane fomain dormation induced by mitochondrial proteins. J. Mol. Biol. *365*, 968–980. https://doi.org/10.1016/j.jmb.2006.10.028.

46. Carranza, G., Angius, F., Ilioaia, O., Solgadi, A., Miroux, B., and Arechaga, I. (2017). Cardiolipin plays an essential role in the formation of intracellular membranes in *Escherichia coli*. Biochim. Biophys. Acta *1859*, 1124–1132. https://doi.org/10.1016/j.bbamem.2017.03.006.

47. Laage, S., Tao, Y., McDermott, A.E., Cegelski, L., Weliky, D.P., and V, P.E.B. (2015). Cardiolipin interaction with subunit c of ATP synthase: solid-state NMR characterization. Biochim. Biophys. Acta *1848*, 260–265. https://doi.org/10.1016/j.bbamem.2014.08.021.

48. Planas-Iglesias, J., Dwarakanath, H., Mohammadyani, D., Yanamala, N., Kagan, V.E., and Klein-Seetharaman, J. (2015). Cardiolipin interactions with proteins. Biophys. J. *109*, 1282–1294. https://doi.org/10.1016/j.bpj.2015.07.034.

49. van Raaij, M.J., Abrahams, J.P., Leslie, A.G., Walker, J.E., Leslie, A.G.W., and Walker, J.E. (1996). The structure of bovine F1-ATPase complexed with the peptide antibiotic efrapeptin. Proc. Natl. Acad. Sci. USA *93*, 6913–6917. https://doi.org/10.1073/pnas.93.14.6913.

50. Amini, A., Raheem, S., Steiner, A., Deeba, F., and Ahmad, Z. (2020). Insect venom peptides as potent inhibitors of *Escherichia coli* ATP synthase. Int. J. Biol. Macromol. *150*, 23–30. https://doi.org/10.1016/j.ijbiomac.2020.02.046.

51. Duncan, A.L., Robinson, A.J., and Walker, J.E. (2016). Cardiolipin binds selectively but transiently to conserved lysine residues in the rotor of metazoan ATP synthases. Proc. Natl. Acad. Sci. USA *113*, 8687–8692. https://doi.org/10.1073/pnas.1608396113.

52. Mühleip, A., McComas, S.E., and Amunts, A. (2019). Structure of a mitochondrial ATP synthase with bound native cardiolipin. Elife *8*, 1–23. https://doi.org/10.7554/eLife.51179.

53. Spikes, T.E., Montgomery, M.G., and Walker, J.E. (2020). Structure of the dimeric ATP synthase from bovine mitochondria. Proc. Natl. Acad. Sci. USA *117*, 23519–23526. https://doi.org/10.1073/pnas.2013998117.

54. Flygaard, R.K., Mühleip, A., Tobiasson, V., and Amunts, A. (2020). Type III ATP synthase is a symmetry-deviated dimer that induces membrane curvature through tetramerization. Nat. Commun. *11*, 5342. https://doi.org/10.1038/s41467-020-18993-6.

55. De Kruijff, B. (1997). Lipids beyond the bilayer. Nature *386*, 129–130. https://doi.org/10.1038/386129a0.

56. Laganowsky, A., Reading, E., Allison, T.M., Ulmschneider, M.B., Degiacomi, M.T., Baldwin, A.J., and Robinson, C.V. (2014). Membrane proteins bind lipids selectively to modulate their structure and function. Nature *510*, 172–175. https://doi.org/10.1038/nature13419.

57. Montecucco, C., Smith, G.A., Dabbeni-sala, F., Johannsson, A., Galante, Y.M., and Bisson, R. (1982). Bilayer thickness and enzymatic activity in the mitochondrial cytochrome c oxidase and ATPase complex. FEBS Lett. *144*, 145–148. https://doi.org/10.1016/0014-5793(82)80588-7.

58. Killian, J.A. (1998). Hydrophobic mismatch between proteins and lipids in membranes. Biochim. Biophys. Acta *1376*, 401–415. https://doi.org/10.1016/S0304-4157(98)00017-3.

59. Arias-Cartin, R., Grimaldi, S., Arnoux, P., Guigliarelli, B., and Magalon, A. (2012). Cardiolipin binding in bacterial respiratory complexes: structural and functional implications. Biochim. Biophys. Acta *1817*, 1937–1949. https://doi.org/10.1016/j.bbabio.2012.04.005.

60. Romantsov, T., Battle, A.R., Hendel, J.L., Martinac, B., and Wood, J.M. (2010). Protein localization in *Escherichia coli* cells : comparison of the membrane proteins ProP, LacY, ProW, AqpZ, MscS, and MscL. J. Bacteriol. *192*, 912–924. https://doi.org/10.1128/JB.00967-09.

61. El Khoury, M., Swain, J., Sautrey, G., Zimmermann, L., Van Der Smissen, P., Décout, J.L., and Mingeot-Leclercq, M.P. (2017). Targeting bacterial cardiolipin enriched microdomains: an antimicrobial strategy used by amphiphilic aminoglycoside antibiotics. Sci. Rep. *7*, 10697. https://doi.org/10.1038/s41598-017-10543-3.

62. Corey, R.A., Pyle, E., Allen, W.J., Watkins, D.W., Casiraghi, M., Miroux, B., Arechaga, I., Politis, A., and Collinson, I. (2018). Specific cardiolipin–SecY interactions are required for proton-motive force stimulation of protein secretion. Proc. Natl. Acad. Sci. USA *115*, 7967–7972. https://doi.org/10.1073/pnas.1721536115.

63. Felício, M.R., Silva, O.N., Gonçalves, S., Santos, N.C., and Franco, O.L. (2017). Peptides with dual antimicrobial and anticancer activities. Front. Chem. *5*, 5. https://doi.org/10.3389/fchem.2017.00005.

64. Horcas, I., Fernández, R., Gómez-Rodríguez, J.M., Colchero, J., Gómez-Herrero, J., and Baro, A.M. (2007). WSXM: a software for scanning probe microscopy and a tool for nanotechnology. Rev. Sci. Instrum. *78*, 013705. https://doi.org/10.1063/1.2432410.

65. Marrink, S.J., Risselada, H.J., Yefimov, S., Tieleman, D.P., and De Vries, A.H. (2007). The MARTINI force field: coarse grained model for biomolecular simulations. J. Phys. Chem. B *111*, 7812–7824. https://doi.org/10.1021/jp071097f.

66. Wassenaar, T.A., Ingólfsson, H.I., Böckmann, R.A., Tieleman, D.P., and Marrink, S.J. (2015). Computational lipidomics with insane: a versatile tool for generating custom membranes for molecular simulations. J. Chem. Theor. Comput. *11*, 2144–2155. https://doi.org/10.1021/acs.jctc.5b00209.

67. de Jong, D.H., Singh, G., Bennett, W.F.D., Arnarez, C., Wassenaar, T.A., Schäfer, L.V., Periole, X., Tieleman, D.P., and Marrink, S.J. (2013). Improved parameters for the martini coarse-grained protein force field. J. Chem. Theor. Comput. *9*, 687–697. https://doi.org/10.1021/ct300646g.

68. Humphrey, W., Dalke, A., and Schulten, K. (1996). VMD: visual molecular dynamics. J. Mol. Graph. *14*, 33–38. https://doi.org/10.1016/j.carbon.2017.07.012.

69. Michaud-Agrawal, N., Denning, E.J., Woolf, T.B., and Beckstein, O. (2011). MDAnalysis: a toolkit for the analysis of molecular dynamics simulations. J. Comput. Chem. *32*, 2319–2327. https://doi.org/10.1002/jcc.

70. Gowers, R.J., Linke, M., Barnoud, J., Reddy, T.J.E., Melo, M.N., Seyler, S.L., Dotson, D.L., Buchoux, S., Kenney, I.M., Beckstein, O., et al. (2016). MDAnalysis : a Python package for the rapid analysis of molecular dynamics simulations MDAnalysis. In Proceedings of the 15th Python in Science Conference, pp. 98–105.

71. Harris, C.R., Millman, K.J., van der Walt, S.J., Gommers, R., Virtanen, P., Cournapeau, D., Wieser, E., Taylor, J., Berg, S., Smith, N.J.,

et al. (2020). Array programming with NumPy. Nature *585*, 357–362. https://doi.org/10.1038/s41586-020-2649-2.

72. Gutiérrez-Sanz, Ó., Natale, P., Márquez, I., Marques, M.C., Zacarias, S., Pita, M., Pereira, I.A.C., López-Montero, I., De Lacey, A.L., and Vélez, M. (2016). H_2-fueled ATP synthesis on an electrode: mimicking cellular respiration. Angew Chem. Int. Ed. Engl. *55*, 6216–6220. https://doi.org/10.1002/anie.201600752.

73. Almendro-Vedia, V.G., Natale, P., Mell, M., Bonneau, S., Monroy, F., Joubert, F., and López-Montero, I. (2017). Nonequilibrium fluctuations of lipid membranes by the rotating motor protein F1FO-ATP synthase. Proc. Natl. Acad. Sci. USA *114*, 11291–11296. https://doi.org/10.1073/pnas.1701207114.

74. Hernansanz-Agustín, P., Choya-Foces, C., Carregal-Romero, S., Ramos, E., Oliva, T., Villa-Piña, T., Moreno, L., Izquierdo-Álvarez, A., Cabrera-García, J.D., Cortés, A., et al. (2020). Na+ controls hypoxic signalling by the mitochondrial respiratory chain. Nature *586*, 287–291. https://doi.org/10.1038/s41586-020-2551-y.

75. Stone, T.J., Buckman, T., Nordio, P.L., and McConnell, H.M. (1965). Spin-labeled biomolecules. Proc. Natl. Acad. Sci. USA *54*, 1010–1017. https://doi.org/10.1073/pnas.54.4.1010.

76. Lanzetta, P.A., Alvarez, L.J., Reinach, P.S., and Candia, O.A. (1979). An improved assay for nanomole amounts of inorganic phosphate. Anal. Biochem. *100*, 95–97. https://doi.org/10.1016/0003-2697(79)90115-5.

77. Yguerabide, J., Schmidt, J.A., and Yguerabide, E.E. (1982). Lateral mobility in membranes as detected by fluorescence recovery after photobleaching. Biophys. J. *40*, 69–75. https://doi.org/10.1016/S0006-3495(82)84459-7.

78. Axelrod, D., Koppel, D.E., Schlessinger, J., Elson, E., and Webb, W.W. (1976). Mobility measurement by analysis of fluorescence photobleaching recovery kinetics. Biophys. J. *16*, 1055–1069. https://doi.org/10.1016/S0006-3495(76)85755-4.

79. Smolyakov, G., Formosa-Dague, C., Severac, C., Duval, R.E., and Dague, E. (2016). High speed indentation measures by FV, QI and QNM introduce a new understanding of bionanomechanical experiments. Micron *85*, 8–14. https://doi.org/10.1016/j.micron.2016.03.002.

80. Chopinet, L., Formosa, C., Rols, M.P., Duval, R.E., and Dague, E. (2013). Imaging living cells surface and quantifying its properties at high resolution using AFM in QI^{TM} mode. Micron *48*, 26–33. https://doi.org/10.1016/j.micron.2013.02.003.

81. Aufderhorst-Roberts, A., Chandra, U., and Connell, S.D. (2017). Three-phase coexistence in lipid membranes. Biophys. J. *112*, 313–324. https://doi.org/10.1016/j.bpj.2016.12.025.

82. Hutter, J.L., and Bechhoefer, J. (1993). Calibration of atomic-force microscope tips. Rev. Sci. Instrum. *64*, 1868–1873. https://doi.org/10.1063/1.1143970.

83. Su, J., Marrink, S.J., and Melo, M.N. (2020). Localization preference of antimicrobial peptides on liquid-disordered membrane domains. Front. Cell Dev. Biol. *8*, 350. https://doi.org/10.3389/fcell.2020.00350.

84. Hess, B., Kutzner, C., Van Der Spoel, D., and Lindahl, E. (2008). Gromacs 4: algorithms for highly efficient, load-balanced, and scalable molecular simulation. J. Chem. Theor. Comput. *4*, 435–447. https://doi.org/10.1021/ct700301q.

85. Bussi, G., Donadio, D., and Parrinello, M. (2007). Canonical sampling through velocity rescaling. J. Chem. Phys. *126*, 014101. https://doi.org/10.1063/1.2408420.

86. Parrinello, M., and Rahman, A. (1981). Polymorphic transitions in single crystals: a new molecular dynamics method. J. Appl. Phys. *52*, 7182–7190. https://doi.org/10.1063/1.328693.

STAR★METHODS

KEY RESOURCES TABLE

REAGENT or RESOURCE	SOURCE	IDENTIFIER
Antibodies		
Polyclonal Anti-F_1 beta	Agrisera	RRID: AB_2063154
Monoclonal Anti F_O b	Cusabio	Lot number L1215A-1
Polyclonal Goat anti rabit IgG secondary antibody	Invitrogen	RRID: AB_1185567
Bacterial and virus strains		
Escherichia coli MG1655	ATCC4	7076
Chemicals, peptides, and recombinant proteins		
1-palmitoyl-2-oleoyl-sn-glycero-3-phosphocholine (POPC)	Avanti	Cat#850457C
1,2-Dioleoyl-sn-glycero-3-phosphoethanolamine (DOPE)	Avanti	Cat#850725P
CL bovine heart	Avanti	Cat#840012P
1-palmitoyl-2-oleoyl-sn-glycero-3-phosphoglycerol POPG	Avanti	Cat#840457P
Polar lipid extract	Avanti	Cat#100600P
16:0-5 Doxyl PC	Sigma Aldrich	CAS# 188004-24-2; 810601P
16:0-16 Doxyl PC	Sigma Aldrich	CAS# 216491-65-5; 810604P
Malachite green hydrochloride	Sigma Aldrich	CAS# 123333-61-9; 213020
Ammonium molybdate	Sigma Aldrich	CAS# 13106-76-8; 277908
Adenosine 5′-triphosphate (ATP)	Sigma Aldrich	CAS# 34369-07-8; A2383
DL-dithiothreitol (DTT)	Sigma Aldrich	CAS# 3483-12-3; D0632
cOmplete™ protease inhibitor cocktail	Sigma Aldrich	4693116001
Methyl sulfonyl fluoride (PMSF)	Thermo Fisher	CAS# 329-98-6; 36978
Deposited data		
EcDBS1R4 3D-CG structure	This study	https://zenodo.org/deposit/7920702
Eshcerichia coli F_O domain structure	PDB Sobti, M et al.[39]	6VWK
Software and algorithms		
NIS-Elements	Nikon	https://www.microscope.healthcare.nikon.com/products/software/nis-elements
JPK Data Processing Software v. 6.0.55	Bruker	https://www.jpk.com/downloads
WSxM	Horcas et al.[64]	http://wsxm.eu/download.html
Matlab	MathWorks	https://www.mathworks.com/
GROMACS v 2016.4 and 2020.3	GNU Library General Public License v2.1 or later	https://doi.org/10.5281/zenodo.3562495
MARTINI 2 force field	Marrink , S. J. et al.[65]	http://www.cgmartini.nl/index.php/downloads
INSANE (INSert membraNE)	Wassenaar, T. A. et al.[66]	http://www.cgmartini.nl/index.php/downloads/tools/239-insane
MARTINIZE	De Jong, D. H. et al.[67]	http://cgmartini.nl/index.php/tools2/proteins-and-bilayers/204-martinize

(*Continued on next page*)

Continued

REAGENT or RESOURCE	SOURCE	IDENTIFIER
Visual Molecular Dynamics (VMD)	Humphrey, W. et al.[68]	https://www.ks.uiuc.edu/Development/Download/download.cgi?PackageName=VMD
MDAnalysis	Michaud-Agrawal, N et al.[69]; Gowers R. J. et al.[70]	https://userguide.mdanalysis.org/stable/installation.html
numpy	Harris C.[71]	https://numpy.org/install/
Graph Pad Prism 5	Dotmatics	https://www.graphpad.com

RESOURCE AVAILABILITY

This study did not generate new unique reagents.

Lead contact

Further information and requests for resources and reagents should be directed to and will be fulfilled by the lead contact, Nuno C. Santos (nsantos@fm.ul.pt).

Materials availability

This study did not generate new materials.

Data and code availability

- All data reported in this paper will be shared by the lead contact upon request.
- All original code has been deposited at Zenodo and is publicly available as of the date of publication. DOIs are listed in the key resources table.
- Any additional information required to reanalyze the data reported in this paper is available from the lead contact upon request.

EXPERIMENTAL MODEL AND STUDY PARTICIPANT DETAILS

Bacteria strains and culture

E. coli MG1655 (ATCC47076) were grown at 37°C in LB medium to an optical density of 0.6 at 620 nm.

METHOD DETAILS

E. coli inner membrane vesicle isolation

Bacteria (*E. coli* MG1655: ATCC47076) were lysed by passing the culture twice through a French press, at 4°C, in PBS 10 mM, pH 7.7, with cOmplete 100 mM, DNase 100 μg/mL and lysozyme 200 μg/mL. The lysate was centrifuged (7000 × *g*, 15 min, 4°C) to get rid of debris and the supernatant was collected. Next, bacterial membranes were obtained by ultracentrifugation of the supernatant (174,000 × *g*, 60 min, 4°C). Outer and inner membranes were separated through centrifugation in a sucrose (36-55%) density gradient (347,000 × *g*, 30 min, 4°C). Inner membranes (with their characteristic brown color) were collected from the 45% sucrose layer and stored at -80°C in a HEPES buffer supplemented with 5% glycerol. To obtain the inner membrane vesicles (IMVs), inner membranes were subjected to 15 intercalated 5 s cycles of bath sonication / incubation in ice.

Peptide

EcDBS1R4 (PMKKKLAARILAKIVAPVW, 95% of purity) was purchased from Peptide 2.0 (Chantilly, VA, USA). Peptide was prepared in filtered Milli-Q H_2O for the measurements and stored at 4°C, protected from light.

Materials

POPC, DOPE, POPG, *E. coli* Polar lipid extract (PLE) and TopFluor-CL were purchased from Avanti Polar Lipids. Lipids were stored at −20°C. Sodium chloride, hydrochloric acid, magnesium chloride, potassium chloride, glucose, glycerol, sucrose, malachite green hydrochloride, ammonium molybdate,

tris(hydroxymethyl)aminomethane (Tris), dibasic potassium phosphate, adenosine 5'-triphosphate (ATP), bovine serum albumin (BSA), DL-dithiothreitol (DTT), n-Dodecyl-β-d-maltoside (DDM), methyl sulfonyl fluoride (PMSF), cOmplete^{TM} protease inhibitor cocktail, TOCL, 5-doxyl palmitoyl PC (5-doxyl PC) and 16-doxyl PC were purchased from Sigma Aldrich. 2-[Methoxy(polyethyleneoxy)propyl]-trimethoxysilane (PEG-silane) was purchased from Gelest. Lysogeny broth (LB) was purchased from Thermo Fisher. Phosphate buffered saline 6.7 mM (Ca^{2+} and Mg^{2+} free, pH 7) was purchasd from HyClone. Ultrapure water was produced from a Milli-Q unit (Millipore; conductivity lower than 18 MΩcm).

F_1F_O purification

F_1F_O ATP synthase was purified from *E. coli* MG1655 cytoplasmic membranes using a multiple column strategy alternating anion exchange with size exclusion chromatography. 1 mg/m F_1F_O-ATP synthase (determined through BSA / UV absorption method) was detergent-extracted from the cytoplasmic membranes through solubilization of the membranes with a rupture buffer (50 mM Tris-HCl (pH 8.0), 20% (v/v) glycerol, 2% (w/v) dodecylmaltoside (DDM)) for 60 min at 4°C under gentle mixing. Non-solubilized membranes were removed by ultracentrifugation (250,000 × *g*, 30 min, 4°C) with a TLA100.4 rotor (Beckman Coulter, CA, USA). The supernatant containing the solubilized membranes was then loaded on a 5 mL anion exchange column (HiPrep XL H 16/10) previously equilibrated with 50 mM Tris-HCl (pH 8), 20 % (v/v) glycerol, 100 mM KC1, 0.05% (w/v) DDM. The column was washed with 1 column volume using a variation of the previous buffer, with 125 mM KCl instead. Bound protein was eluted with a 125 - 300 mM KCl gradient in 10 column volumes at a flow rate of 1 mL/min and a collected fraction volume of 1 mL. The F_1F_O ATP synthase complex containing fractions were identified by Western blot analysis using specific antibodies against the beta-subunit (F_1) and the b-subunit (F_O) of the complex. Identified fractions were pooled and loaded onto a size exclusion chromatography column (HiPrep 26/60 Sephacryl S-300 HR, GE) previously equilibrated with 50 mM Tris-HCl (pH 8), 20 % (v/v) glycerol, 100 mM KC1, 0.05% (w/v) DDM at a flow rate of 0.5 mL/min to separate the F_1F_O-ATP synthase complex (~530 kDa) from other proteins present in the sample. Proteins were eluted from the column with the same buffer and the collected fractions and the F_1F_O-ATP synthase complex containing fraction were identified by Western blot analysis. The purified ATP synthase was stored at -80°C.[72]

Reconstitution of F_1F_O ATP synthase into proteoliposomes

The purified F_1F_O-ATP synthase of *E. coli* was reconstituted, together with the desired lipid mixtures into proteoliposomes by rapid dilution.[73] 100 μL of purified F_1F_O-ATP synthase (~ 0.2 mg/mL) were incubated with 80 μL of lipid (20 mM; lipid to protein molar ratio ~ 50,000:1) for 45 min on ice and rapidly diluted to a volume of 3 mL with 67 mM PBS- (Ca^{2+} and Mg^{2+} free, pH 8). Proteoliposomes carrying the F_1F_O-ATP synthase (F_1F_O-SUVs) were collected by ultracentrifugation (30 min at 346,000 × *g* with an MLA 80 rotor, Beckman), resuspended in 100 μL of HEPES 10 mM, pH 7.4, 150 mM NaCl and size-homogenized by 10 intercalated 5 s cycles of incubation in ice / bath-sonication.

EPR of lipid vesicles

EPR experiments were carried out on a Bruker EMX spectrometer at 9 GHz, at a constant temperature of 25°C. POPC:CL (4:1) small unilamellar vesicles (2 mM) were obtained by probe tip ultrasonication for 10 min.[74] The spin labels (0.75% mol of total lipid composition) were added to the dry lipids before vesicle formation to obtain a symmetrical distribution of probes in the two leaflets. 5-doxyl palmitoyl PC (5-doxyl PC) and 16-doxyl PC were the spin labelled lipids chosen. The different position of the probe along the acyl chain probes the local motional profiles near the polar headgroup (5-doxyl PC), or at the end of the hydrophobic chain (16-doxyl PC). The τ_c of 5-doxyl PC is proportional to the outermost separation between the spectral extrema, $2A_{max}$, whereas the τ_c of 16-doxyl PC were calculated by the semi-empirical formula previously established: $\tau_c = 6.5 \times 10^{-10}\ \Delta H_0\ [(h_0/h_{-1})^{1/2} - 1]$, where ΔH_0 is the width of the central line in Gauss, and h_0 and h_{-1} are the heights of the mid-field and high-field lines, respectively.[75] $2A_{max}$, ΔH_0, h_0 and h_{-1} were obtained from the first derivative of each absorption spectrum.

ATP hydrolysis activity

The ATPase activity of inner membrane vesicles and F_1F_O reconstituted proteoliposomes was assessed by monitoring the amount of inorganic phosphate released during the hydrolysis of ATP. Inorganic phosphate concentrations were measured by means of an adapted version of the colorimetric protocol described by Lanzetta et al.[76] 7 μL of 1 mM (lipid concentration) inner membrane vesicles or F_1F_O-reconstituted proteoliposomes

were incubated for 15 min in Tris-HCl pH 8.0 in a 96 well plate in the absence and presence of peptide, at room temperature (final lipid concentration of 1 mM). ATP was added to a final concentration of 0.5 mM and incubated for 15 min at room temperature. 100 μL of reaction buffer (Tris-HCl60 μM, pH 8, KCl 60 μM, $MgCl_2$6 μM , DTT1 μM, BSA 6 μg/mL dissolved in ultrapure H_2O) was added to each well and the mixture was incubated at 37°C for 30 min. The color solution of malachite green/ammonium molybdate was finally added and absorbance at 660 nm was read using a microplate reader Multiskan FC Thermo Fisher Scientific spectrometer.[76]

Preparation of supported lipid bilayers

Supported lipid bilayers (SLBs) for confocal microscopy were produced by rupture of small unilamellar vesicles (SUVs) to a PEG-silane cushion. Briefly, 1 mM of tip sonicated vesicles containing 0.5% of TopFluor-CL were incubated in the presence of 1 M $MgCl_2$ and 1 M NaCl for 30 min. Then, the supported bilayers were thoroughly rinsed with HEPES 10 mM, pH 7.4, 150 mM NaCl, to remove remaining non-deposited vesicles and excess of salt.

On the other hand, SLBs for AFM measurements were prepared by SUVs deposition on a mica support, as previously described. Briefly, 500 μL of a SUVs suspension of 100 μM was deposited in the presence of 1.5 μL $CaCl_2$ 1 M on a freshly cleaved mica substrate previously glued to a glass coverslip. The sample was incubated for 1 h at room temperature in a highly humid chamber to avoid desiccation. After incubation, the sample was rinsed 10 times with HEPES 10 mM, pH 7.4, 150 mM NaCl.

Confocal microscopy

Lateral diffusion of supported lipid bilayers was evaluated in the absence and presence of peptide using fluorescence recovery after photobleaching (FRAP). FRAP experiments were performed using a Nikon Ti-E inverted microscope equipped with a Nikon C2 confocal scanning confocal module. An area of approximately 300 μm^2 of the SLB (carrying 0.5% mol of Top Fluor-CL) was photobleached with a 488 nm continuous laser (Sapphire). Fluorescence recovery was recorded in time steps of 5 s. The fluorescence recovery curves were fitted to[77]:

$$f(t) = \frac{f(0)+f(\infty)\cdot(t/t_{1/2})}{1+(t/t_{1/2})} \quad \text{(Equation 1)}$$

where $f(t)$ is the time normalized fluorescence intensity, $F(t)/F_0$, being F_0 the fluorescence intensity just before photobleaching, $f(0)$ the fluorescence intensity just after photobleaching the sample, $f(\infty)$ the normalized maximum fluorescence intensity and $t_{1/2}$ the time required for the bleached fluorescence to achieve 50% of the full recovery value. The lateral diffusion coefficient, D, is related to $t_{1/2}$ as[78]:

$$D = \frac{\omega^2}{4\cdot t_{1/2}}\beta \quad \text{(Equation 2)}$$

where β is a parameter that accounts for the beam shape and the bleaching extent, and ω is the bleached radius.[77]

Atomic force microscopy

Atomic force microscopy was performed using a JPK Nanowizard IV (JPK instruments, Berlin, Germany). Bilayers were imaged in quantitative imaging (QI mode), a recent innovation in which the apparatus modulates the z-piezo to perform a fast force curve on each pixel of the image.[79,80] This avoids lateral friction and allows for better control of the tip force during measurements. The QI mode enables several mechanical properties to be calculated from the force applied and the tip-sample separation. Throughout the imaging, the maximum applied force was 200 pN, in order not to affect the sample structure.[81] Images were obtained with a resolution of 256 × 256 pixels, at a scan rate of 1 Hz. AFM measurements were performed at room temperature, which varied from 22 to 25°C. Before the measurements, cantilever spring constants were quantified by the thermal noise method,[82] and cantilever sensitivity was measured by performing a force curve on a clean freshly cleaved mica surface, in HEPES buffer. For the used qpBioAC CB2 AFM probes, the spring constant and sensitivity values obtained were 0.06-0.18 N/m and 7.6 ± 1.2 nm/V, respectively. A fixed area of 10 × 10 μm^2 was followed for kinetic topography changes after peptide addition. Topographical images were analyzed with first or second level flattening, using the WSxM software[64] and JPK Data Processing Software v. 6.0.55. The topography profiles were evaluated by several cross sections on the supported lipid bilayers images.

Simulation setups

Membrane models were constructed with the aid of the *insane* script[66] (for the details of the simulated membrane models, see Table 1). The coarse-grained MARTINI structure of EcDBS1R4 was obtained using the Martinize script,[67] using as a template the structure described in.[32] A coarse-grained model of the F_O motor —the transmembrane domain— of a bacterial F_1F_O ATP synthase was built from the cryo-EM structure of the ATP synthase from *E. coli* (PDB ID: 6VWK),[39] using the *Martinize* script. The F_O motor was introduced in a lipid bilayer with a 940:1 lipid-to-protein ratio. For the systems in which peptide was added, a lipid-to-peptide ratio of 40:1 was used, unless otherwise specified. For the peptide adsorption-equilibration the following protocol was used[83]: the first and last backbone bead particles of each peptide were restrained in the *xy*-plane with a harmonic potential of 3000 kJ mol^{-1} nm^{-2}, to prevent untimely peptide–peptide associations that might have led to the formation of unwanted pre- equilibrium peptide aggregates. Furthermore, a harmonic restraint in z (5000 kJ mol^{-1} nm^{-2}) was applied on the peptides, pulling them to a 2.5 nm distance from the bilayer center. This second restraint aimed at preventing dissociation into the aqueous phase whilst allowing the peptides to rotate parallel to the bilayer plane to optimally face the bilayer.

To investigate the effect of the peptide interacting with only one leaflet we prepared a treadmill belt-like lipid bilayered micelle (*i.e.,* bicelle) model. Peptide insertion in a lipid bilayer would cause lateral pressure asymmetries that would turn the system highly unstable. Thus, the false-bilayer nature of the bicelle allows a rapid dissipation of lateral pressure asymmetries. The bicelle model composed of 1478 lipid molecules and x/y dimension ratio of 2.5. After we performed an equilibration with a Parrinello-Rahman semiisotropic pressure coupling with compressibility in the x/y direction turned off. The dimensions of the system cage were then expanded in the x plane. This caused the invasion of water molecules to fill the void space, which in turn caused the bilayer to adopt curved ends, formed by the polar headgroups, to minimize the contact of the solvent with the hydrophobic tails (forming the bicelle). Consequently, the bicelle lost its periodicity in the x axis. To this bicelle, peptide molecules were added to one side, using the same protocol as in the bilayers. The mobility of the peptide was restricted to a central 'corral' of the bicelle through a flat-bottomed position restraint with a harmonic potential of 300 kJ $mol^{-1}nm^{-2}$ and 7 nm of radius, parallel to the short axis of the bicelle. Lipid-to-peptide ratio was initially 12:1 inside the corral. In addition, to maintain membrane buckling under control, an additional flat-bottomed position restraint of 1000 kJ $mol^{-1}nm^{-2}$ was applied to the phosphate beads, whose mobility was vertically restricted to a slab of 4.4 nm of height, with the reference set in the mean height of the membrane.[83]

Force field and simulation details

Coarse-grained molecular dynamic simulations were performed using GROMACS (versions 2016.4 and 2020.3)[84] and MARTINI2 force fields.[65] Simulations were performed using periodic boundary conditions with constant number of particles, constant pressure, and constant temperature (*NpT* ensemble) with a 20-fs time step. The temperature was maintained at 300 K using the v-rescale thermostat and a coupling constant τ_t of 1.0 ps.[85] Unless otherwise stated (*i.e.* bicelle systems), pressure was coupled semi-isotropically with a Parrinello-Rahman barostat at 1 bar with compressibility of 3×10^{-4} bar^{-1} a coupling constant τ_p of 12 ps.[86] Coulombic and van der Waals non-bonded interactions were cut-off at an interparticle distance of 1.1 nm and translated by a constant to be zero at the cut-off. Coulombic interactions followed reaction-field electrostatics with a dielectric constant of 15.

Simulation analysis

Analysis algorithms were programmed in Python, using MDAnalysis[70,69] and NumPy.[71] Plots were generated using Matplotlib and Graph Pad Prism 5 softwares. Visual Molecular Dynamics software (VMD) was used for visualization and generation of occupancy maps (VolMap tool), with a resolution of 2 Å.[68] Data are presented as time-weighted average values, with 95% confidence intervals estimated by a 10k- resample bootstrapping of the time-weighted averaging.

QUANTIFICATION AND STATISTICAL ANALYSIS

Graphs and statistics were prepared and analyzed using GraphPad Prism 5 software and the python packages nump, scipy and scikits.bootstrap to obtain the 95% of confidence intervals.